Supporting Information

for

The diatom frustule-based Mn_2SiO_4@C@SiO_2 multilayer-structure composite as a high-performance anode electrode material for lithium-ion batteries

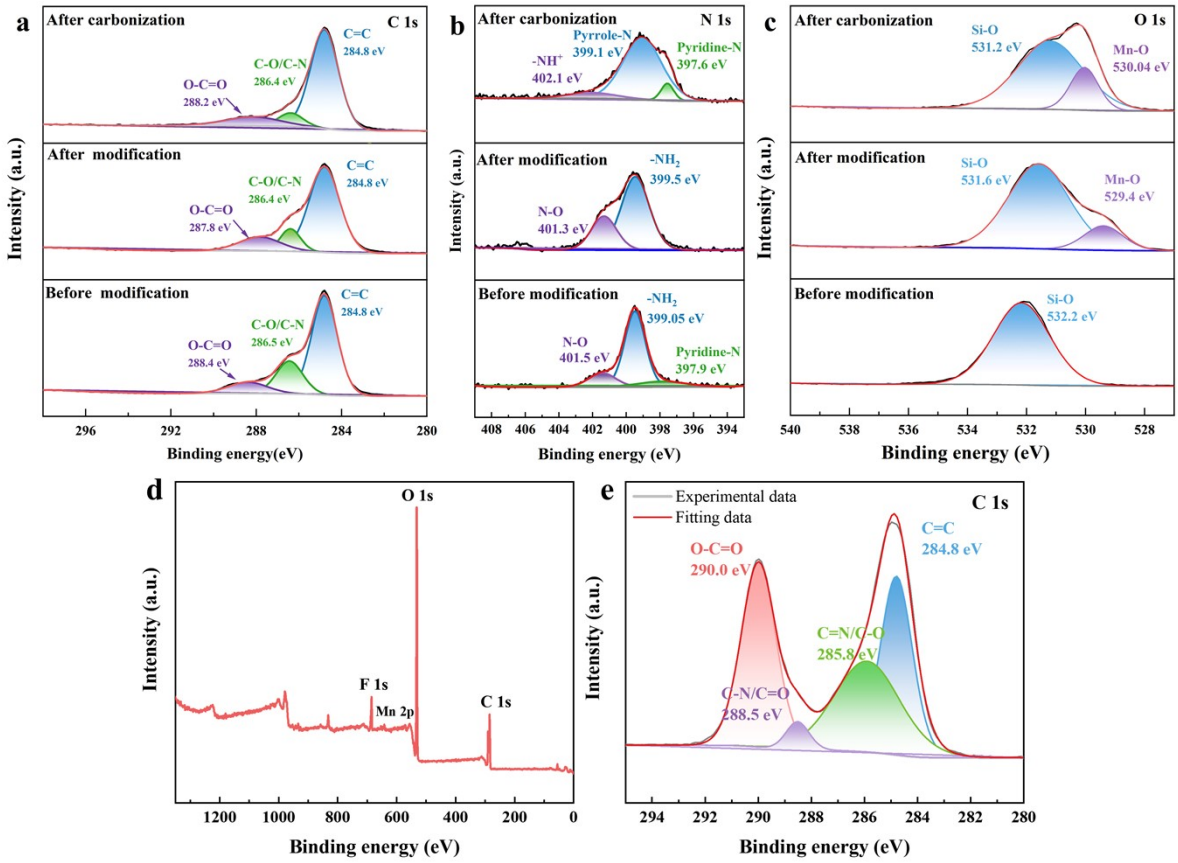

Fig. S1. XPS spectra and fitted results of DBS, AFD-Mn-40, and AFD@C-Mn-40. (a) C 1s, (b) N 1s, (c) O 1s, (d) survey, and (e) C1s of AFD-Mn-40 after 200 cycles.

The high-resolution N 1s spectrum shows the presence of pyrrole N in AFD@C-Mn-40. Pyrrole N can often be used as a functional and active site to accelerate Li^+ diffusion, which has positive significance for improving the electrochemical properties of composites. The source of N may be the biomass of diatom frustules or $-NH_2$ in APTES. The O 1s spectrum shows characteristic peaks of Si–O bonds at 532.2 eV (DBS), 531.6 eV (AFD-Mn-40), 531.2 eV (AFD@C-Mn-40), and 529.4 eV (AFD-Mn-40). The spectral peak of the Mn-O bond at 530.04 eV (AFD@C-Mn-40) and the characteristic peaks of the C-C bond (284.8 eV), C-O/C-N (286.4 eV), and O-C=O (288.2 eV) are displayed in the C 1s spectrum. The C1s spectral results of the electrode material after cycling show that the content of O-C=O

increases significantly, which may be caused by the addition of conductive carbon black and NMP. The C1s spectral results of the electrode material after 200 cycles show that the content of O-C=O increases significantly, which may be caused by the addition of conductive carbon black and NMP. In the full spectrum of the XPS spectrum of the electrode material after 200 cycles, the characteristic peaks of Si 2p almost disappear, and the data before Si 2p fitting after 200 cycles are more chaotic than the characteristic peaks before the cycling, which corresponds to the conversion of SiO_2 to amorphous Si after the electrochemical cycle.

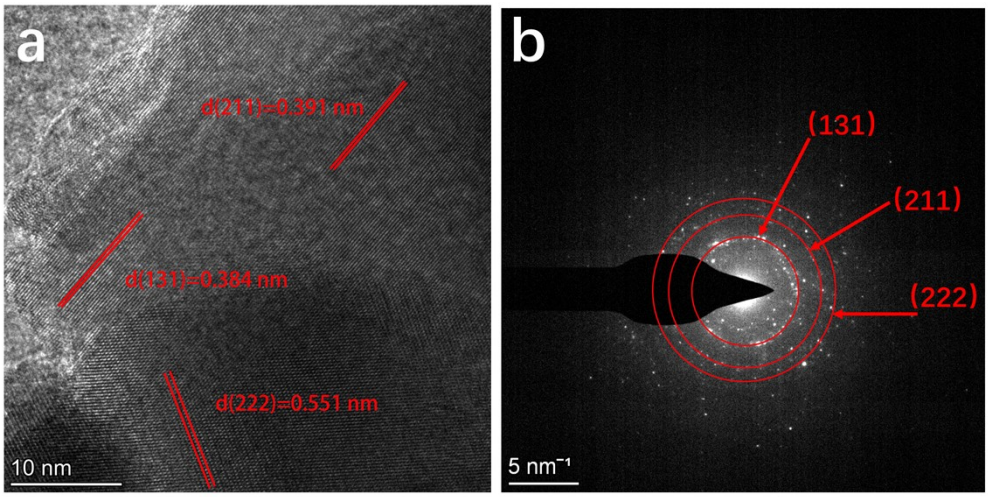

Fig. S2. (a) HRTEM images and (b) SAED images of the area I of AFD@C-Mn-40 (indicated in Fig. 3(c)).

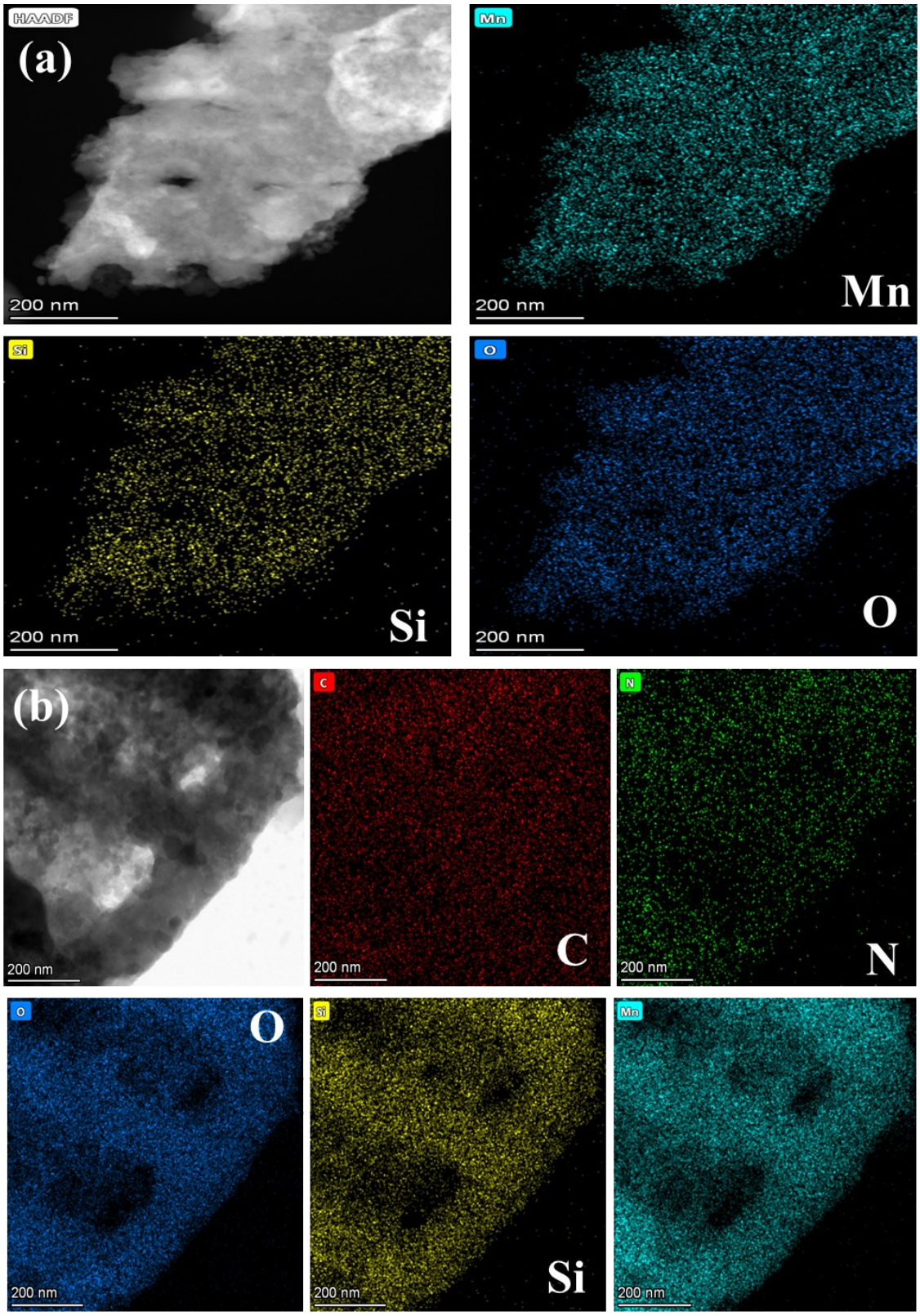

Fig. S3. TEM-EDX images of (a)AFD@C-Mn-20 and (b) AFD@C-Mn-40.

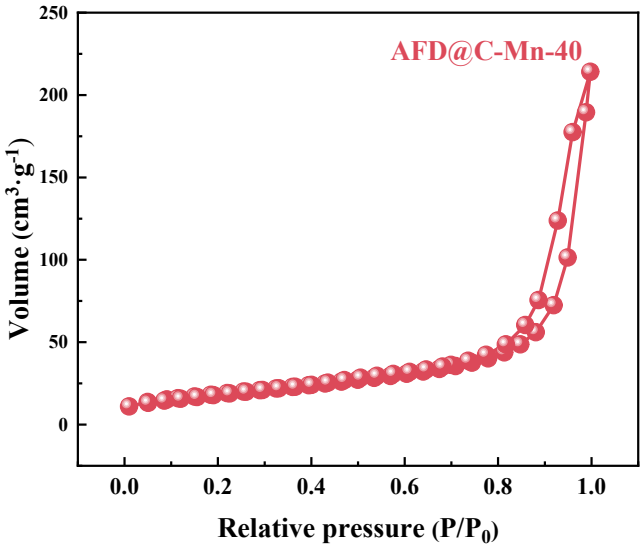

Fig. S4. N_2 adsorption/desorption isotherm curve of AFD@C-Mn-40.

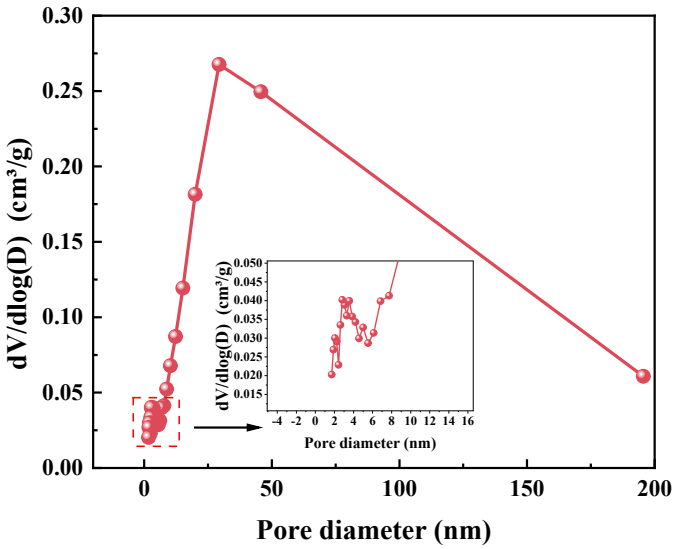

Fig. S5. Pore size distribution curve of AFD@C-Mn-40.

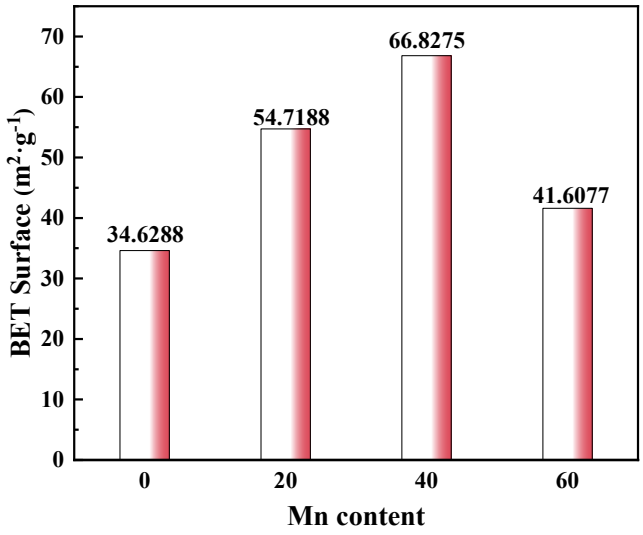

Fig. S6. BET surface areas of the composites with different Mn contents.

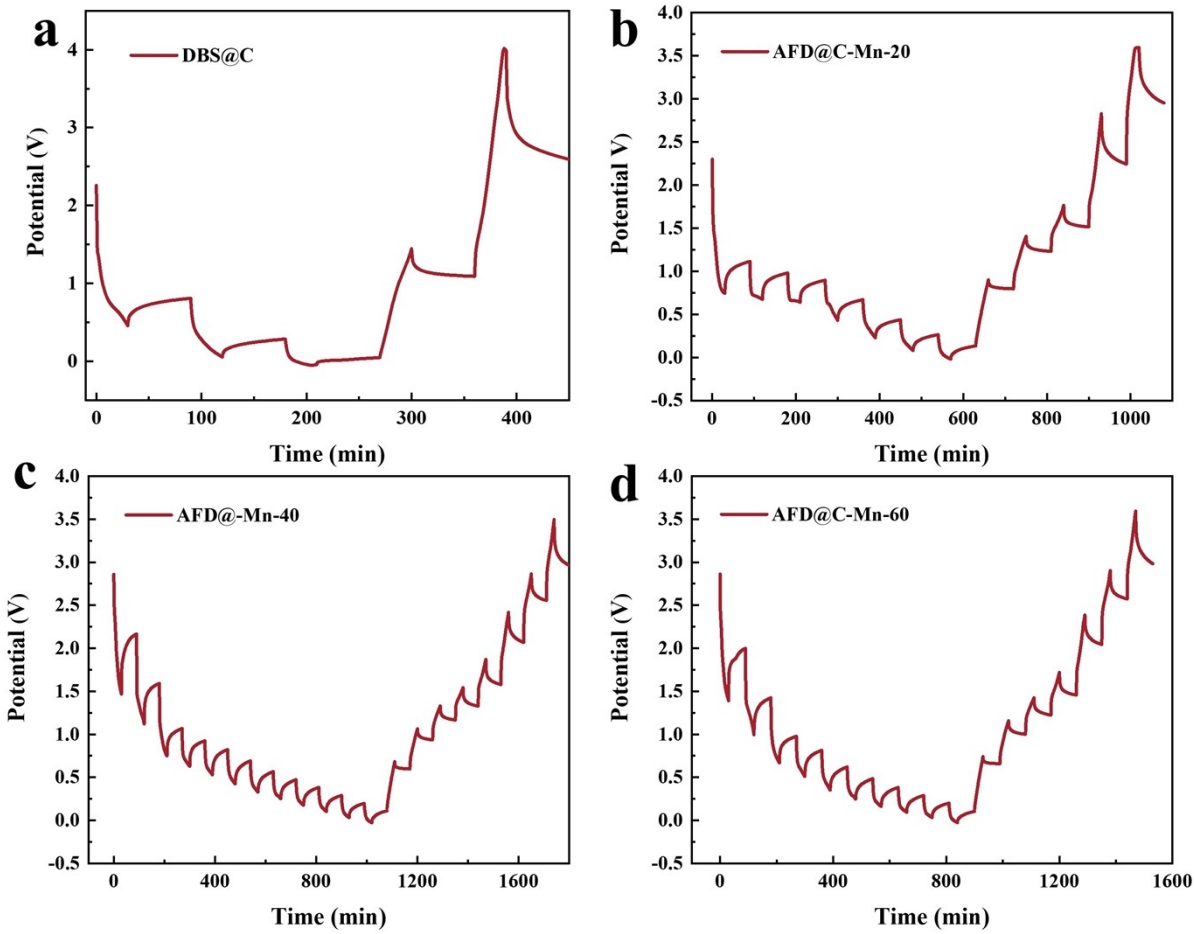

Fig. S7. GITT test map spectrum of AFD@C-Mn materials.

According to the GITT results of the AFD@C-Mn electrode material, D_{Li^+} is calculated according to Fick's second law, and Fick's second law is solved to obtain the solution of the lithium-ion diffusion coefficient:

$$D = \frac{4}{\pi}\left(\frac{iV_m}{Z_{Li}FS}\right)\left[\frac{\left(\frac{dE}{d\delta}\right)}{\left(\frac{dE}{d\sqrt{t}}\right)}\right]^2$$

where i is the current (mA), Z_{Li+} is the charge number of Li^+(1), F is the Faraday charge constant (96485 C/mol), S is the contact area between the electrode and the electrolyte, the unknown parameters are dE/dδ, which is the slope of the Coulomb titration curve, dE/d √ t

represents the relationship between the potential and time when the applied current is small enough, and dE/d √ t is linear. The calculation formula is further simplified as follows:

$$D = \frac{4}{\pi\tau}\left(\frac{n_m V_m}{S}\right)^2\left[\frac{\Delta E_s}{\Delta E_t}\right]^2$$

where τ is the duration of the current pulse, n_m is the number of moles, V_m is the molar volume, S is the electrode/electrolyte contact area, ΔE_s is the total voltage change caused by the pulse, and ΔE_t is the voltage change of constant current charge/discharge. The calculation results are shown in Table S2.

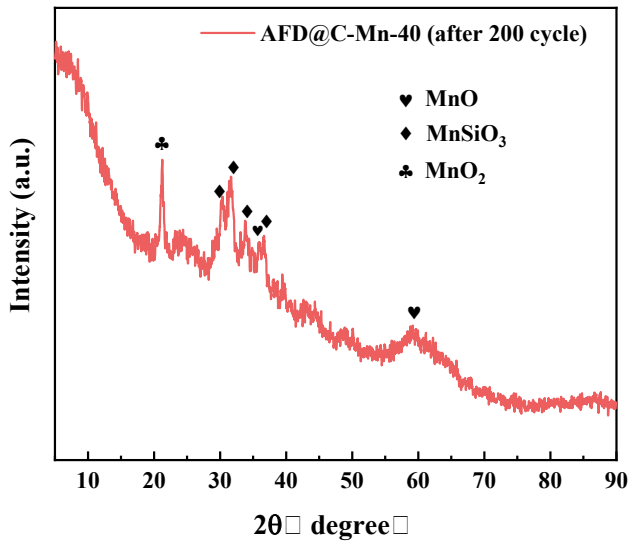

Fig. S8. XRD patterns of the AFD@C-Mn-40 electrode material after 200 cycles.

Table S1. BET specific surface area/micropore diameter/surface area of the composite.

	BET specific surface area ($m^2 \cdot g^{-1}$)	**micropore diameter (nm)**	**surface area (m^2/g)**
DBS@C	34.6228	18.9484	29.9321
AFD@C-Mn-20	54.7188	19.5955	55.9803
AFD@C-Mn-40	66.8275	19.8232	67.4598
AFD@C-Mn-60	41.6077	23.6030	43.9652

Table S2. Parameters obtained from the EIS results of different electrodes.

	D_{Li^+}(cm·s^{-1})	σ
DBS@C	2.96×10^{-16}	1260.14
AFD@C-Mn-20	6.89×10^{-16}	826.21
AFD@C-Mn-40	1.21×10^{-15}	621.82
AFD@C-Mn-60	7.61×10^{-16}	786.06

Table S3. The content of each sample in the composite material.

	Si (%)	Mn(%)	C(%)	H_2O(%)
DBS@C	26.72%	--	23.87	5.79
AFD@C-Mn-20	16.31%	41.55%	9.63	1.46
AFD@C-Mn-40	11.29%	51.44%	10.06	2.23
AFD@C-Mn-60	7.94%	51.49%	10.52	3.22

Table S4. Comparison of the electrochemical properties of similar silicate anodes.

Sample name	Mass ratio	Discharge specific capacity	Current density	Reference
Mn_2SiO_4@C@SiO_2	**7：2：1**	**1112 mAh·g^{-1}（100 cycles）**	**100 mA·g^{-1}**	**Our work**
Mn_2SiO_4/C	8:1:1	345 mAh·g^{-1} (100 cycles)	200 mA·g^{-1}	[1]
Co_2SiO_4	7.5:2:0.5	650 mAh·g^{-1}(100 cycles)	160 mA·g^{-1}	[2]
Zn_2SiO_4@NC	7:2:1	685 mAh·g^{-1} (100 cycles)	100 mA·g^{-1}	[3]
Zn_2SiO_4	7:2:1	520.2 mAh·g^{-1} (50 cycles)	100 mA·g^{-1}	[4]
MnO/Mn_2SiO_4@C	7:2:1	639 mAh·g^{-1} (200 cycles)	500 mA·g^{-1}	[5]
Mn_2SiO_4/GO	7:2.5:0.5	1015 mAh·g^{-1} (150 cycles)	200 mA·g^{-1}	[6]

Table S5. The average specific discharge capacity ($mAh \cdot g^{-1}$) of the composite during 10 cycles with different currents.

	200 $mA \cdot g^{-1}$	**500 $mA \cdot g^{-1}$**	**1 $A \cdot g^{-1}$**	**2 $A \cdot g^{-1}$**	**100 $mA \cdot g^{-1}$**
DBS@C	149.97	90.16	58.15	34.12	187.58
AFD@C-Mn-20	345.8	240.23	189.05	141.82	436.94
AFD@C-Mn-40	592.96	486.36	411.35	307.15	719.10
AFD@C-Mn-60	489.01	405.45	354.49	291.5	594.27

Reference

1. Y.-Y. Wang, T. Li, Y.-X. Qi, R.-L. Bai, L.-W. Yin, H. Li, N. Lun ,Y.-J. Bai, Electrochim. Acta 186 (2015) 572-578.
2. F. Mueller, D. Bresser, N. Minderjahn, J. Kalhoff, S. Menne, S. Krueger, M. Winter ,S. Passerini, Dalton Trans. 43 (2014) 15013-15021.
3. F. Liu, S. Liu, J. Meng, F. Xia, Z. Xiao, Z. Liu, Q. Li, J. Wu ,L. Mai, Nano Energy 73 (2020) 104758.
4. S. Zhang, M. Lu, Y. Li, F. Sun, J. Yang ,S. Wang, Mater. Lett. 100 (2013) 89-92.
5. H. Wei, Z. Xia ,D. Xia, ACS Appl. Mater. Interfaces 9 (2017) 43657-43664.
6. J. Zhu, C. Tang, Z. Zhuang, C. Shi, N. Li, L. Zhou ,L. Mai, ACS Appl. Mater. Interfaces 9 (2017) 24584-24590.